Quantum geometry and the stability of fractional Chern insulators

Mathi Raja, Bartholomew Andrews, and Michael Zaletel
Department of Physics, University of California at Berkeley, Berkeley, California 94720, USA
(Dated: August, 2023)

The stability of fractional Chern insulators (FCIs) is yet to be rigorously understood and in this paper, we make advances in understanding how single-particle stability quantities such as band dispersion, topology, and geometry influence the stability of many-body FCI states. Specifically, it has been demonstrated that single-particle measures such as the gap-to-width ratio (flatness parameter), fluctuations of the Berry curvature, and the trace inequality saturation measure, correlate with metrics for FCI stability. We reproduce many of the results in the literature relating band geometry to FCI stability, such as the relationship between the many-body gap, trace inequality saturation measure, and the strength of the 3rd-nearest neighbor hopping in the zero quadratic model[1, 2]. Using an infinite density matrix renormalization group algorithm, we research the many-body spectrum and find that we can stabilize an FCI in the zero quadratic model, which is verified by determining its charge pumping, entanglement entropy, and spectral flow.

I. INTRODUCTION

As the original example of a topological phase of matter with fractional excitations, the fractional quantum Hall effect has motivated significant research efforts, and the possible applications in quantum metrology and computing are exciting. Normally, fractional quantum Hall states require low temperature/high magnetic fields to be realized, however, in the two-dimensional lattice generalization known as fractional Chern insulators (FCIs), fractional quantum Hall states have the potential to be realized at zero magnetic field and at room temperature[3–5]. Furthermore, FCIs introduce more parameters to tune, such as the first Chern number leading to interesting novel phases. This makes FCIs especially appealing for applications like topological quantum computing, so in the past decade, significant theoretical interest has focused on FCIs [6].

Throughout the literature, the stability of FCIs has been shown to be related to the resemblance to Landau Levels, depending on band flatness, Berry curvature, and more recently the Fubini-Study (FS) metric is also shown to play a role in determining their stability [7]. To investigate this further, this paper focuses on the zero-quadratic model (ZQM), as this model has been found to be able to specifically tune certain measures of FCI stability without affecting other quantities related to band geometry.

Thus, the rest of this paper will focus on providing background to, and seeking to answer the question of how, to best characterize the FCI stability. For example, whether the single-particle band gap being large enough compared to interaction strength and bandwidth allows for stability [6] or if the (defined below) trace inequality saturation measure (TISM) becoming closer to 0 (fully saturated) influences stability more strongly [1]. As for any fractional quantum Hall state, many-body interactions are crucial, and we will employ infinite density matrix renormalization group (iDMRG) simulations restricted to an infinite cylinder geometry using tensor network methods to understand the effects of this in our FCI model [8].

II. SINGLE-PARTICLE SPECTRUM

A. Zero-Quadratic Model Band Structure

Motivated as an extension of the Harper-Hofstadter (HH) model (see Appendix A for detail on the HH model), we introduce a 3rd nearest-neighbor hopping to arrive at the zero-quadratic model (ZQM) [1]:

$$H = -t_1 \sum_{\langle ij \rangle_1} e^{\mathrm{i}\theta_{ij}} c_i^\dagger c_j - t_3 \sum_{\langle ij \rangle_3} e^{\mathrm{i}\theta_{ij}} c_i^\dagger c_j + V \sum_{\langle ij \rangle_1} \rho_i \rho_j + \text{H.c.} \tag{1}$$

Note that the indices for t and $\langle ij \rangle_a$ denotes the a^{th} nearest-neighbor hopping, t_i are hopping strengths for the respective hoppings and $c_i^\dagger$ and c_j symbolize creation and annihilation operators under second quantization. $\rho_i = c_i^\dagger c_i$ is the density operator and V symbolizes the interaction strength, but in the single-particle case, we keep $V = 0$. We also have a magnetic flux of $n_\phi = \frac{p}{q} = \frac{B}{\phi_0}$ where $\phi_0 = \frac{h}{e}$ (flux quantum). This magnetic flux is manifested in the Peierl's phase, θ_{ij} (see Appendix A). As shown in [1] and explained in Appendix A, ZQM allows us to observe an FCI which does not necessarily recover the Landau Level Hamiltonian in the weak-field/continuum limit.

Diagonalizing this Hamiltonian, we get the following example band structure at the parameters $t_3 = -\frac{1}{4}$ and $n_\phi = \frac{1}{5}$ shown in Fig. 1 (see Appendix B for more detailed derivation).

B. Topological Invariants

To understand the topological nature of our bands, we must compute the necessary topological invariant: Chern numbers (as motivated by the TKNN formula showing the Hall conductivity of a system is a topological invariant) [9]. Although the first Chern number is defined as the integration of the Berry curvature over the Brillouin Zone, we cannot use a normal finite difference method

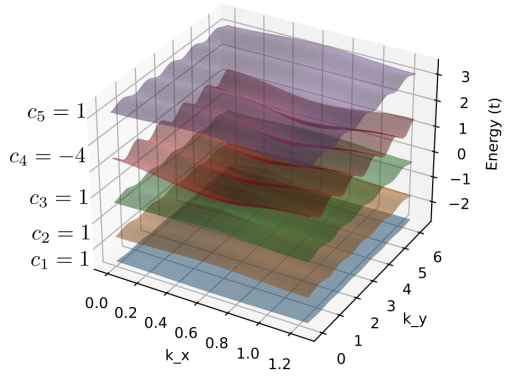

FIG. 1: Band structure for the single-particle ZQM model at $t_3 = -\frac{1}{4}$ and $n_\phi = \frac{1}{5}$. The Chern numbers for each respective band are shown to the left of the plot and the magnetic Brillouin zone (ranging from 0 to $2\pi/5$ in the k_x direction and from 0 to 2π in the k_y direction) is discretized by 100 in each direction.

with the formula above to compute the Berry curvature because we cannot efficiently fix the local gauge in which the eigenvectors are smoothly differentiable for us to integrate. Thus, we use the following formula from [10] where we can sum over discretized plaquettes in the Brillouin Zone (identified at each k where k_i represents the i^{th} corner in a counter-clockwise fashion starting from k in a certain plaquette)

$$c_n = \frac{1}{2\pi} \sum_{\mathbf{k} \in \text{BZ}} \text{Im} \ln \left[U^{(n)}_{\mathbf{k}_1 \to \mathbf{k}_2} U^{(n)}_{\mathbf{k}_2 \to \mathbf{k}_3} U^{(n)}_{\mathbf{k}_3 \to \mathbf{k}_4} U^{(n)}_{\mathbf{k}_4 \to \mathbf{k}_1} \right] \tag{2}$$

with $U^{(n)}_{\mathbf{k}_\alpha \to \mathbf{k}_\beta} \equiv \frac{\langle \mathbf{u}_{n,e,\mathbf{k}_\alpha} | \mathbf{u}_{n,e,\mathbf{k}_\beta} \rangle}{|\langle \mathbf{u}_{n,e,\mathbf{k}_\alpha} | \mathbf{u}_{n,e,\mathbf{k}_\beta} \rangle|}$ known as link variables [10]. From this, we can now calculate our corresponding Chern numbers which, for example, given conditions from Fig 1, yields Chern numbers of 1 for all the bands except the 4th from the bottom, which has a Chern number of -4. To arrive at a fractional quantum Hall state in an FCI, we require flat and topologically non-trivial bands. For simplicity, we take our lowest band in the ZQM model which will have a Chern number of 1.

To further showcase the topological nature of the Chern number, we can also plot the Wilson loops, the product of Berry phases along a periodic loop in one direction along the Brillouin Zone as seen in Fig. 2 and Fig. 3.

The Wilson loops have a winding number around the Brillouin Zone identical to the magnitude of the respective band's Chern number and the sign of the Chern number describes its orientation. For our band structure, a band with Chern number 1 creates a Wilson loop along k_x of winding number 1 while for a band with Chern number -4, a Wilson loop of winding number 4 and flipped orientation.

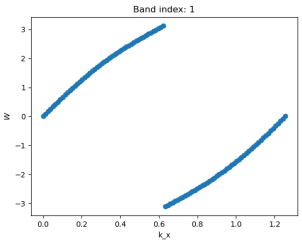

FIG. 2: Wilson loop for $c_1 = 1$ band

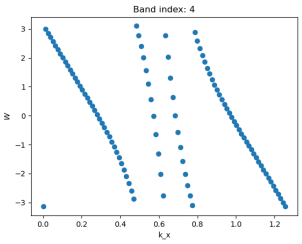

FIG. 3: Wilson loop for $c_4 = -4$ band

C. Quantum Geometry

In quantum Hall physics (Landau levels), magnetic translation operators follow a certain Lie algebra known as the Girvin-Macdonald-Platzmann (GMP) algebra. We thus motivate paying attention to non-topological, geometric quantities due to the "band geometry hypothesis", which implies that the more accurately the GMP algebra is reproduced, the more stable the FQHE states are on a lattice. [7].

We introduce band geometry through the quantum geometric tensor (QGT) given as [11, 12]:

$$\mathcal{R}^s_{ab} = [\partial_{k_a} \langle u^s(k)|] \mathcal{Q}^s(k) [\partial_b |u^s(k)\rangle] \tag{3}$$

where $\mathcal{Q}^s(k) = 1 - \sum_{r \neq s} |k^r\rangle \langle k^r|$. Intuitively, the QGT can be thought of as a distance of Bloch eigenvectors on a Bloch sphere. The QGT can further be broken into its real and imaginary components represented by the Fubini-Study (FS) metric (g^s_{ab})and the Berry curvature (Ω^s_{ab}) respectively:

$$\begin{aligned} \text{Re}(\mathcal{R}^s_{ab}) = g^s_{ab} = \frac{1}{2}(&\langle \partial_{k_a} u^s(k) | \partial_{k_b} u^s(k) \rangle \\ &- \langle \partial_{k_a} u^s(k) | u^s(k) \rangle \langle u^s(k) | \partial_{k_b} u^s(k) \rangle + a \leftrightarrow b) \end{aligned} \tag{4}$$

$$\begin{aligned} -2\text{Im}(\mathcal{R}^s_{ab}) = \Omega^s_{ab} = i(&\langle \partial_{k_a} u^s(k) | \partial_{k_b} u^s(k) \rangle \\ &- \langle \partial_{k_b} u^s(k) | \partial_{k_a} u^s(k) \rangle \end{aligned} \tag{5}$$

We have already addressed the Berry curvature in Sec II B, but the FS metric additionally introduces a natural notion of distance in the single-particle Hilbert space from the evolution of single-particle eigenstates. From these quantities derived from the QGT, it is shown that these two inequalities based on the quantum geometric tensor must be satisfied [1, 2, 7]:

$$\text{Det} g(k) \geq \frac{1}{4} |\mathcal{B}(k)|^2, \quad \text{Tr} g(k) \geq |\mathcal{B}(k)|, \tag{6}$$

where $\mathcal{B}(k)$ is the Berry curvature and we can define:

$$\mathcal{D} = \mathrm{Det}g(k) - \frac{1}{4}|\mathcal{B}(k)|^2, \quad \mathcal{T} = \mathrm{Tr}g(k) - |\mathcal{B}(k)|. \quad (7)$$

Note that the minimization of the trace inequality saturation measure (TISM), denoted by $\mathcal{T}$ in Eq 7, is a stronger condition than the minimization of the determinant inequality saturation measure (DISM), denoted by $\mathcal{D}$ in Eq 7. It has been hypothesized that small Berry curvature fluctuations (constant Berry curvature) and smaller TISM will support a more stable FCI. According to the work by Parameswaran et al., the mapping between Hamiltonians in the lowest Landau level and Hamiltonians in Chern bands can be understood through the operator algebras in each [13]. The trace inequality saturation measure (TISM) can be used to determine how well the GMP algebra is reproduced in the case when Chern bands are already energetically flat with a large gap and flatness parameter, as well as low Berry curvature fluctuations [14]. Specifically, the TISM being satisfied means the algebra of the projected densities of eigenstates in a Chern band is the same as the algebra of the continuous Landau level case [13].

Thus, we can integrate the TISM over the Brillouin zone to get the quantity $\langle\mathcal{T}\rangle$. Comparing it to the different FCIs we can create by tuning t_3, we get Fig. 4. Compared to [1], our plot shows the same dependence of $\mathcal{T}(k)$ on t_3.

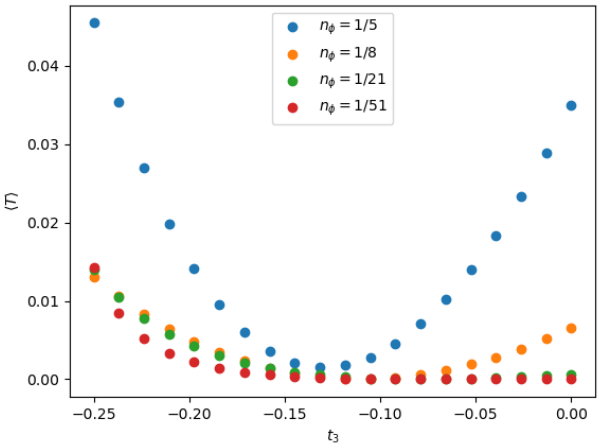

FIG. 4: Plot showing the TISM being satisfied as n_ϕ becomes smaller. Data is taken at various $n_\phi = 1/q$ values. The line at $t_3 = -0.25$ corresponds to the zero-quadratic point and $t_3 = 0$ corresponds to the Hofstadter model.

D. Utility of the ZQM

When attempting to understand the influence of band geometry in FCI stability using the Harper-Hofstadter model, it is not possible to change $\langle\mathcal{T}\rangle$ without directly affecting other quantities such as the Berry flatness and thus we employ the ZQM. As shown in Fig 5, in the ZQM, we have a different relationship where the Berry curvature fluctuations have a roughly linear dependence from $t_3 \approx -0.25$ to $t_3 \approx 0$. In the Hofstadter model, the Berry curvature fluctuations and TISM both follow an exponential trend with flux density and one cannot be independently modified without significantly disturbing the other. Thus it is advantageous to use the ZQM to isolate the effects of $\langle\mathcal{T}\rangle$ on FCI stability. Similarly, in the ZQM, we can tune the trace inequality saturation measure by simply changing t_3, while in the Hofstadter model, the only way to modify the TISM is to adjust the flux density, n_ϕ (as n_ϕ becomes smaller we approach the continuum limit). As an added benefit, we also have particular values of hopping where we see that there's no Landau level continuum limit (e.g. $t_1 = 1$ and $t_3 = -\frac{1}{4}$) in the ZQM, which helps us to eliminate the influence of a continuum limit entirely.

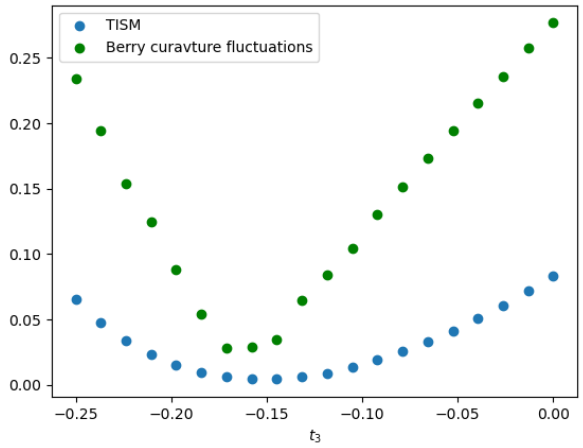

FIG. 5: Plot showing the relationship between fluctuations of the Berry curvature and $\langle\mathcal{T}\rangle$ when varying t_3.

III. MANY-BODY SYSTEM

A. Methods

To include many-body effects, we must now introduce a non-zero interaction strength, V, and consider interaction behavior. To start, we restrict interactions to a nearest-neighbor density-density interaction potential for fermions and on-site contact interaction for bosons. To numerically simulate the interaction, we use an infinity density matrix renormalization group algorithm (iDMRG) implemented via TeNPy [8]. As a high-level overview of the algorithm, it iteratively finds a represen-

tation of the ground state using a Schmidt decomposition of the intended system into two half-infinite cylinders and truncates the dimension at a certain parameter known as the bond dimension, χ_{MPS}. The quantum many-body system is represented as a superposition of its bases using tensors as coefficients called a matrix product state (MPS). The DMRG algorithm then variationally minimizes the ground-state energy by using an engine to adjust neighboring tensors while keeping other tensors fixed. After stepping through a specified number of times or until a threshold is reached, a new matrix product state is created with new tensor coefficients which is then again passed through the engine. Eventually, this process will converge the wave function (represented by the MPS) to the ground state [8]. The Schmidt decomposition also allows us to directly access eigenvalues of the reduced density matrix of states and thus we can obtain the von Neumann entanglement entropy as well as the entanglement spectrum (ϵ_α) between the two halves of the cylinders via $e^{-\epsilon_\alpha} = \Lambda_\alpha^2$, where Λ_α is a Schmidt coefficient for some α [15].

B. Many-body results

In a many-body FQHE state, we can observe the quantization of the Hall conductivity given as:

$$\sigma_H = \frac{e^2}{2\pi h} \int d\Phi_x d\Phi_y \nabla \times \mathcal{A}(\Phi_x, \Phi_y), \tag{8}$$

where Φ_x is the phase induced by a flux going through the cylinder an electron travels on and $\mathcal{A}(\Phi_x, \Phi_y)$ is the Berry connection of the ground state wavefunction on a torus. The iDMRG algorithm allows us to compute this quantity efficiently by first calculating the Berry Phase ($\gamma_n = \int_{\mathcal{C}} d\mathbf{R} \cdot \mathcal{A}_n(\mathbf{R})$) and using that to find the conductivity. For a $c = 1$ band, there is exactly one unit of charge pumped across the boundary after one flux quantum. Thus, for a FQHE state, we must require ν flux insertions for one unit of charge pumped since $\sigma_H = \nu c \frac{e^2}{h}$ and we attempt to check this.

Using the iDMRG algorithm we attempt to create a FCI using the ZQM (at values $t_1 = 1$ and $t_3 = -\frac{1}{4}$) and check it by monitoring the charge pumping, as well as the entanglement spectral flow. For a boson system, we use a system size of 4×4 with periodic boundary conditions which allows us to specify magnetic unit cells of size 4×1. We choose to simulate a $\nu = \frac{1}{2}$ filling FQHE state and choose $n_\phi = \frac{1}{4}$ which allows us to fill our system with two particles. For a fermion system, we use a system size of (3, 6), again with periodic boundary conditions in the y-direction. We choose to now simulate a $\nu = \frac{1}{3}$ filling FQHE state and choose $n_\phi = \frac{1}{3}$, which allows for two particles again. Running the algorithm on both of these scenarios, we get the following plots in Fig 6, Fig 7 and Fig 8, Fig 9. To generate these plots, we used a $\chi_{\text{MPS}} = 50$ with $\chi_{\text{MPO}} = 8$.

As our charge pumping plots (Fig 6 and Fig 8) show the required fractionalized charge for a FQHE state, we see that our ZQM model stabilizes an FCI. This is further solidified by looking at the spectral flow (Fig 7 and Fig 9) with $U(1)$ charge eigenvalues dropping by 1 after and original entanglement being recovered after $1/\nu$ flux insertions (note we took sufficiently small step sizes so that the flow is adiabatic).

IV. CONCLUSIONS

Throughout this project, we have developed the background to understand the single-particle indicators, which influence FCI stability such as quantum geometric quantities like Berry curvature, the quantum geometric tensor, and the trace inequality saturation measure. We concentrated on investigating the zero quadratic model as we were able to tune the TISM independently of other single-particle properties and also demonstrated that the ZQM has the ability to host FCIs. In future work, we can use the ZQM to help understand many-body indicators of stability. For example, one such way of doing this is finding the critical V (interaction energy) in order to have a FCI similar to as done in [3]. Finally, the influence of symmetry in FCI models has also been hypothesized to influence stability, for example, in the ZQM model defined earlier, the interactions obey a C_4 symmetry, however, in real fractional quantum hall systems, electrons don't necessarily interact with a C_4 symmetry but rather a continuous symmetry and understanding the transition/differences between these two symmetries poses an interesting question.

ACKNOWLEDGMENTS

We acknowledge support from the Physics Innovators initiative (Pi^2) hosted by the Department of Physics, University of California at Berkeley.

Appendix A: Peierl's Phase, magnetic unit cells, and the Harper-Hofstadter Model

We assume the tight-binding approximation and attempt to adapt the Hubbard model with nearest-neighbor hopping:

$$H = t_1 \sum_{\langle ij \rangle_1} c_i^\dagger c_j + \text{H.c.} \tag{A1}$$

to include the effects of the lattice structure and the magnetic flux.

In a general Hofstadter tight-binding Hamiltonian, we introduce a uniform magnetic field B perpendicular to the 2D lattice such that the flux per lattice plaquette is $\phi = Ba^2 = \frac{p}{q}\phi_0$ where $\phi_0 = h/e$ is the magnetic flux

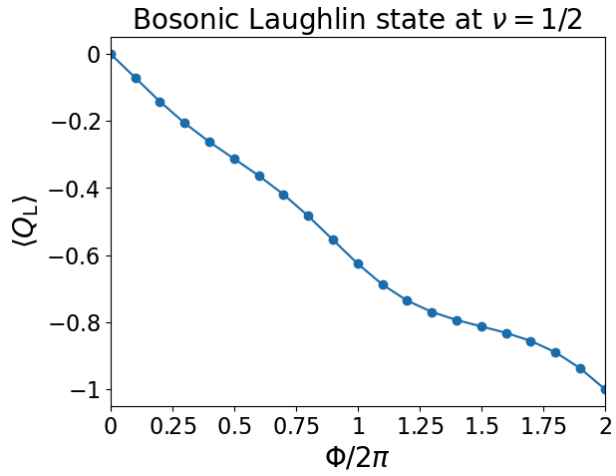

FIG. 6: Charge pumping for the bosonic Laughlin state in the lowest band of the ZQM.

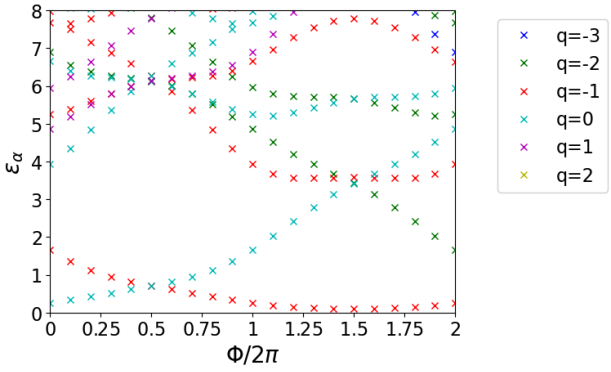

FIG. 7: Spectral flow for the bosonic Laughlin state in the lowest band of the ZQM.

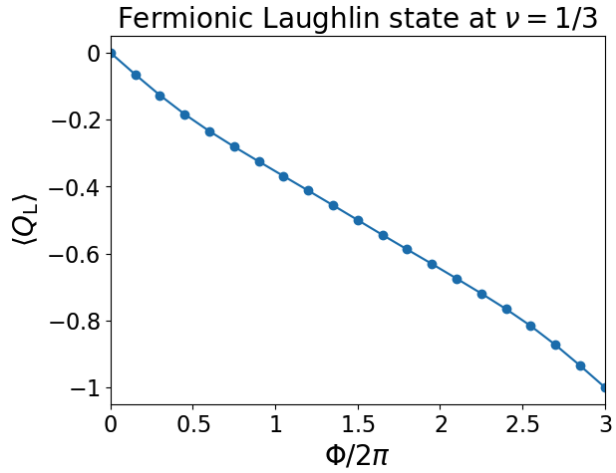

FIG. 8: Charge pumping for the fermionic Laughlin state in the lowest band of the ZQM.

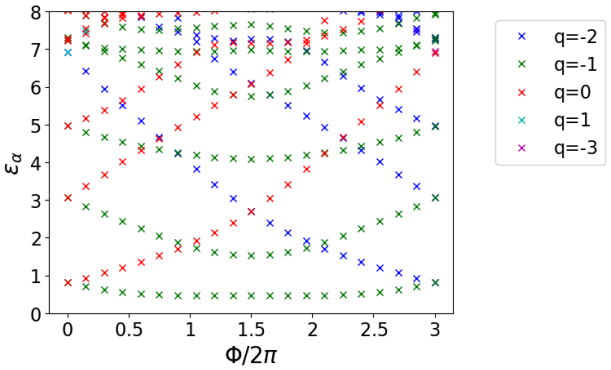

FIG. 9: Spectral flow for the fermionic Laughlin state in the lowest band of the ZQM.

quantum and p and q are coprime integers (but we only consider the case $p = 1$ for simplicity). In units of $\hbar/e = 1$, we see $\phi = a^2/l^2$ is dimensionless. We also define magnetic length as $l = \sqrt{\frac{\hbar}{eB}}$.

In a 2D lattice, the analogy of the Aharanov-Bohm phase charged particles usually experience due to the magnetic field flux is given by the Peierl's phase, defined as:

$$\theta_{ij} = \frac{2\pi}{\Phi_0} \int_i^j A \cdot dl$$

where

$$\mathbf{A} = \begin{bmatrix} 0 \\ Bx \\ 0 \end{bmatrix} \quad \text{such that} \quad \nabla \times A = B.$$

In a tight-binding model, the number of flux quanta per plaquette, ϕ, is related to the lattice curl of the phase factor by the following equation where the total flux through the lattice is $\Phi = \Phi_0 \sum_{m,n} \phi_{m,n}$ with $\Phi_0 = hc/e$ being the magnetic flux quantum:

$$\begin{aligned} \boldsymbol{\nabla} \times \theta_{m,n} &= \Delta_x \theta^y_{m,n} - \Delta_y \theta^x_{m,n} \\ &= \theta^y_{m+1,n} - \theta^y_{m,n} - \theta^x_{m,n+1} + \theta^x_{m,n} \end{aligned} \tag{A2}$$

Note the RHS is just the sum of phases around a loop in some plaquette so we can also write it as a closed loop phase (the second to last equality uses Stokes theorem here and $\phi_{m,n}$ is the magnetic flux in plaquette (m,n)).:

$$\frac{q}{\hbar} \int_{\text{unit cell}} \mathbf{A} \cdot \mathrm{d}\mathbf{l} = 2\pi \frac{q}{h} \int_{\mathrm{S}} \mathbf{B} \cdot \mathrm{d}\mathbf{s} = 2\pi \phi_{m,n}$$

Under the influence of a magnetic field, we must generalize our translation operators as such to involve the

Peierl's phase:

$$T_a = \sum_m e^{i\theta(a(m))} c^\dagger_{m+e_a} c_m$$

These operators don't commute but satisfy:

$$T_x T_y = e^{i\phi} T_y T_x.$$

Since these are unitary, we can write them in terms of generators $T_a = e^{iK_a}$ which satisfy $[K_x, K_y] = i\phi$.

To resolve any ambiguity due to the non-commutativity of the translation operators, we define a translation of (j,k) as $T_x^j T_y^k + T_y^k T_x^j$. This results in our Brillouin zone being shifted to a magnetic Brillouin zone to comply with the adjusted translation operators. For some k by l lattice unit cell, the phase then takes the form $e^{-ikl\Phi}(T_x^M)^k(T_y^M)^l = (T_y^M)^l(T_x^M)^k$ so the smallest super-cell for which $[(T_x^M)^k, (T_y^M)^l] = 0$ is given when $kl\Phi = 2\pi p\frac{kl}{q} \neq 2\pi v, v \in \mathbb{Z}$, so we require that $kl = q$. In our case, we will take by convention to always let the magnetic unit cell extend q in the x-direction and 1 cell in the y-direction.

Going back to our tight-binding model, for a single particle restricted to a 2D square lattice system under the influence of a magnetic field, we must include the Peierl's phases, and our Hamiltonian is now given by:

$$H = t_1 \sum_{\langle ij\rangle_1} e^{\mathrm{i}\theta_{ij}} c_i^\dagger c_j + \text{H.c.},$$

finally, we can add interactions using a density-density interaction to get the interacting Harper-Hofstadter Hamiltonian:

$$H = t_1 \sum_{\langle ij\rangle_1} e^{\mathrm{i}\theta_{ij}} c_i^\dagger c_j + V \sum_{\langle ij\rangle_1} \rho_i \rho_j + \text{H.c.} \tag{A3}$$

Appendix B: Computing the ZQM band structure

We can now take a look at the Zero Quadratic Model Hamiltonian:

$$H = -t_1 \sum_{<ij>_1} e^{\mathrm{i}\theta_{ij}} c_i^\dagger c_j - t_3 \sum_{<ij>_3} e^{\mathrm{i}\theta_{ij}} c_i^\dagger c_j + \frac{V}{2} \sum_{<ij>_1} \rho_i \rho_j + \text{H.c.}$$

We look at the single-particle model, so we set $V = 0$. Attempting to determine the band structure, we look at the eigenvalue equation $H\Psi_{mn} = E\Psi_{mn}$ in momentum space. Thus, we use the ansatz $\Psi_{mn} = e^{ik_x m} e^{ik_y n}\psi_m$ for $0 \leq k_y < 2\pi$ and $0 \leq k_x q < 2\pi$ due to boundary conditions and the modified magnetic unit cell, we also see that $\Psi_{m,n+1} = \Psi_{m,n}$ and $\Psi_{m+q,n} = \Psi_{m,n}$. Substituting the Peierls phase as well as our wave ansatz acting on our eigenvalue equation, we get (skipping simplifications):

$$E\psi_m = C^*\psi_{m-2} + B^*\psi_{m-1} + A\psi_m + B\psi_{m+1} + C\psi_{m+2}$$

for substitutions: $C = -t_3 e^{i2k_x}$, $B = -t_1 e^{ik_x}$, and $A = -2(t_1\cos(2\pi n_\phi m + k_y) + t_3\cos(4\pi n_\phi m + 2k_y))$. From here, we can write our Hamiltonian in a matrix form and diagonalize this to find the band structure.

Appendix C: Effective Landau Levels from weak-field Harper-Hofstadter Hamiltonian

Substituting for translation operators in the Harper-Hofstadter Hamiltonian, we get:

$$H_{\text{TB}} = -\sum_{j,k} t_{jk}(T_x^j T_y^k + T_y^k T_x^j) + \text{H.c.}$$

looking at NN (nearest neighbor) hopping Hamiltonian:

$$H_{\text{NN}} = -t_{10}(T_x + T_x^\dagger) - t_{01}(T_y + T_y^\dagger)$$

if we have C_4 symmetry ($t_{01} = t_{10} = t$), we reduce this to:

$$H_{NN} = -2t\cos(K_x) - 2t\cos(K_y)$$

Rescaling the operators again, using $\sqrt{\phi}P_\alpha = K_\alpha$ for ϕ dependence, we get:

$$H = -4 + \phi(K_x^2 + K_y^2) + O(\phi^2).$$

We can then rewrite K in terms of mechanical momentum, since K is just mechanical momentum but discretized over some lattice constant a instead of $\hbar$ so $K_\alpha = (a/\hbar)\pi_\alpha$ and $P_\alpha = (l/\hbar)\pi_\alpha$ for $\phi P_\alpha = K_\alpha$, we can rewrite first order effective H as:

$$H_{eff} = \phi(P_x^2 + P_y^2),$$

which is isomorphic to the Landau level Hamiltonian given by $H = (\pi_x^2 + \pi_y^2)/2m^*$ where $m^* = \hbar^2/(2a^2)$ and π_i are the mechanical momentum operators [1].

[1] David Bauer, Spenser Talkington, Fenner Harper, Bartholomew Andrews, and Rahul Roy. Fractional Chern insulators with a non-Landau level continuum limit. Phys. Rev. B, 105:045144, Jan 2022.

[2] Rahul Roy. Band geometry of fractional topological insulators. Phys. Rev. B, 90:165139, Oct 2014.

[3] Bartholomew Andrews, Titus Neupert, and Gunnar Möller. Stability, phase transitions, and numerical breakdown of fractional chern insulators in higher chern bands of the hofstadter model. Phys. Rev. B, 104:125107, Sep 2021.

[4] Titus Neupert, Luiz Santos, Claudio Chamon, and Christopher Mudry. Fractional quantum Hall states at zero magnetic field. Phys. Rev. Lett., 106:236804, Jun 2011.

[5] Evelyn Tang, Jia-Wei Mei, and Xiao-Gang Wen. High-temperature fractional quantum Hall states. Phys. Rev. Lett., 106:236802, Jun 2011.

[6] Emil J. Bergholtz and Zhao Liu. Topological flat band models and fractional chern insulators. International Journal of Modern Physics B, 27(24):1330017, 2013.

[7] T. S. Jackson, Gunnar Möller, and Rahul Roy. Geometric stability of topological lattice phases. Nature Communications, 6(1):8629, November 2015.

[8] Johannes Hauschild and Frank Pollmann. Efficient numerical simulations with Tensor Networks: Tensor Network Python (TeNPy). SciPost Phys. Lect. Notes, page 5, 2018. Code available from `https://github.com/tenpy/tenpy`.

[9] Qian Niu, D. J. Thouless, and Yong-Shi Wu. Quantized hall conductance as a topological invariant. Phys. Rev. B, 31:3372–3377, Mar 1985.

[10] Takahiro Fukui, Yasuhiro Hatsugai, and Hiroshi Suzuki. Chern numbers in discretized brillouin zone: Efficient method of computing (spin) hall conductances. Journal of the Physical Society of Japan, 74(6):1674–1677, 2005.

[11] Ran Cheng. Quantum geometric tensor (fubini-study metric) in simple quantum system: A pedagogical introduction. 12 2010.

[12] David Bauer, T. S. Jackson, and Rahul Roy. Quantum geometry and stability of the fractional quantum hall effect in the hofstadter model. Phys. Rev. B, 93:235133, Jun 2016.

[13] S. A. Parameswaran, R. Roy, and S. L. Sondhi. Fractional chern insulators and the W_∞ algebra. Phys. Rev. B, 85:241308, Jun 2012.

[14] Siddharth A. Parameswaran, Rahul Roy, and Shivaji L. Sondhi. Fractional quantum hall physics in topological flat bands. Comptes Rendus Physique, 14(9):816–839, 2013. Topological insulators / Isolants topologiques.

[15] Adolfo G. Grushin, Johannes Motruk, Michael P. Zaletel, and Frank Pollmann. Characterization and stability of a fermionic $\nu = 1/3$ fractional chern insulator. Phys. Rev. B, 91:035136, Jan 2015.